A&A manuscript no.
(will be inserted by hand later)

Your thesaurus codes are:
2 (12.03.3; 12.12.1)

ASTRONOMY AND ASTROPHYSICS

January 7, 2000

Clustering of galaxies at faint magnitudes

J.U. Fynbo[1,2], **W. Freudling**[2,3], **and P. Møller**[2]

[1] Institute of Physics and Astronomy, Århus University, DK-8000 Århus C., Denmark
[2] European Southern Observatory, Karl-Schwarzschild-Straße 2, D-85748, Garching bei München, Germany
[3] Space Telescope – European Coordinating Facility, Karl-Schwarzschild-Straße 2, D-85748, Garching bei München, Germany

Received 28 May 1999 / Accepted 21 December 1999

Abstract. Significant uncertainties exist in the measured amplitude of the angular two-point correlation function of galaxies at magnitudes $I \approx 26$ and fainter. Published results from HST and ground-based galaxy catalogs seem to differ by as much as a factor of 3, and it is not clear whether the correlation amplitude as a function of magnitude increases or decreases in the faintest magnitude bins. In order to clarify the situation, we present new results from both ground-based and HST galaxy catalogs. The angular two-point correlation function as a function of limiting R and I magnitudes was computed from a galaxy catalog created from the Hubble Deep Field - South (HDF-S) WFPC2 image. The measured amplitudes of the correlation at an angular separation of 1 arcsec are consistent with those measured in the Northern counter part of the field. The flanking fields (FF fields) of the Hubble deep fields were used to extend the magnitude range for which we compute correlation amplitudes towards brighter magnitude bins. This allows easier comparison of the amplitudes to ground based data. The ESO NTT Deep Field catalog was used to measure the correlation at similar magnitudes from ground based data. We find that the measured correlation from both the HST and ground based samples are consistent with a continuously decreasing clustering amplitude down to the faintest magnitude limits. Finally, the newly measured correlation amplitudes as a function of magnitude limit were compared to previously published measurements at larger separations. For this comparison, the correlation function was approximated by a power law with an index of 0.8. The scatter in the correlation amplitudes is too large to be explained by random errors. We argue that the most likely cause is the assumption that the shape of the correlation function does not depend on the magnitude limit.

Key words: Cosmology : observations – Cosmology : large scale structure of Universe

1. Introduction

The angular correlation function of galaxies $w(\theta)$ is still the most commonly used tool for investigating the evolution of clustering at high redshift . While a more direct measurement of the two point correlation is significantly more powerful (see e.g. Le Fèvre et al. 1996), its computation requires deep magnitude limited redshift surveys, which currently are not feasable at the faintest reachable magnitude limits. By contrast, the angular correlation function can easily be computed from photometric galaxy catalogs alone. With the availability of the Northern Hubble Deep Fields (HDF-N, Williams et al. 1996), the angular correlation function has been computed to an R magnitude of 29 (Villumsen et al. 1996, hereafter VFC, Colley et al. 1996). These studies suggest that the amplitude of the correlation function continuously decreases with the magnitude limit of the sample over a magnitude range of more than 10 magnitudes down to the faintest magnitude limits probed so far. The amplitude at an angular separation of one arcsec, $w(1'')$, seems to follow closely a power law $w(1'') \propto 10^{-0.27R}$(e.g. Brainerd et al. 1995).

Despite the apparent simplicity of computing the angular correlation function, a significant controversy has arisen about the magnitude limits at which the correlation function flattens. Measuring the correlation amplitude at a separation of 1 arcmin, Brainerd & Smail (1998) found that the correlation amplitude reaches a minimum for samples with limiting I magnitude of about 23 and stays flat for even deeper magnitude limited samples. On the other hand, the deeper HDF-N measurements at a separation of 1 arcsec found a continuously decreasing clustering amplitude down to the faintest magnitude limits. This discrepancy could be due to a number of different reasons such as biased field selection, different redshift selection through differences in the bandpasses, systematic errors in the determination of the clustering amplitude (e.g. due to gradients in the sensitivity of the detector), or simply random fluctuations in the correlation amplitudes. However, it could also mean a true discontinuity of the shape and/or amplitude of the correlation function at a magnitude of $I \approx 26$ or $R \approx 27$.

Before suggesting the existence of a discontinuity of the correlation amplitudes, several tests of the results should be carried out. First of all, both the ground based results and the HDF-N results should be verified by independent samples. Secondly, any apparent discontinuity should be tested with a single sample which covers the relevant magnitude range. Up to now, available ground based have not been not deep enough to over-

Send offprint requests to: J.U. Fynbo
Correspondence to: jfynbo@ifa.au.dk

lap with the HDF results, which are only available for magnitudes fainter than $R \approx 26$. The current work addresses both of these points. We have used the southern HDF field to obtain an independent verification of the previous HDF-N results. In addition, we have used the "flanking fields" of the Northern and Southern HDFs (Williams et al. 1998) to derive a catalog over a larger area and thus allowing us to compute the $w(\theta)$ at brighter magnitudes from an HDF-like sample. Finally, we have used a sample of galaxies detected in a deep ground based image, the so-called ESO NTT deep field (Arnouts et al. 1999) to compute $w(\theta)$ from ground-based data at faint magnitudes. The combined data sets allow us to derive correlation amplitudes from both HST and ground based data at identical magnitude bins, and thereby search for discontinuities in the correlation amplitudes as a function of magnitude.

In Sect. 2, we present the results from the HDF fields which include the Northern HDF, the Southern HDF and the flanking fields. In Sect. 3, we present new results from the ESO NTT deep field. In Sect. 4, we investigate the correlation amplitude as a function of magnitude by combining the new data with previous estimates in the literature. Finally, in Sect. 5, we discuss the results and present our conclusions.

2. HDF samples

2.1. HDF South : The galaxy catalog

We used the "drizzled" HDF-S images distributed by the *Space Telescope – European Coordinating Facility* archive. The galaxy catalog was generated using the SExtractor program (Bertin & Arnouts 1996). The catalog of Clements & Couch (1996) was used by VFC to compute $w(\theta)$ from the HDF-N images. In order to be able to compare our results with the results obtained from the HDF-N we use the exact same extraction parameters as input to SExtractor as those described in Clements & Couch. We use a minimum object extraction area of 30 pixels and a detection threshold of 1.3σ above the background. As a detection image we use a master frame calculated as the sum of the combined images taken with the F606W and F814W filters, which are similar to the R and I passbands respectively. As a detection filter we use a top-hat filter of 30 connected pixels. We checked the reliability of the extraction parameters by comparing the master frame with the output object image, which SExtractor optionally provides. We could not detect any tendency to find spurious objects in the vicinity of bright objects. The useful part of the combined mosaic frames are different between the HDF-N and HDF-S because the WFPC2 fields of view are slightly rotated relative to the mosaiced image which is aligned with the north/south direction. Therefore, we re-defined for each of the WF2, WF3 and WF4 CCDs useful areas from visual inspection of the master frame. Fig.1 shows the chosen areas. Only objects detected within the shown boundaries were used in the analysis. In order to excluded stars from the galaxy catalog we set an upper limit to the neural network star parameter in the output SExtractor catalog of 0.98, which excluded 20 objects. This is consistent with

Table 1. Survey data for the deep fields used in the determination of the twopoint correlation function

field	Area	I(complete)	R(complete)
	arcsec^2		
HDF-S	3.7	28.0	28.5
HDF-S FF	33.2	25.5	-
HDF-N	4.2	28.0	28.5
HDF-N FF	8.7	25.5	-
NTT	4.4	25.5	25.5

the number of stars expected for a field with the galactic latitude and depth as the HDF-S. Also we exclude saturated stars found by visual inspection from the galaxy catalog. There are not very bright stars in the HDF-S so we did not mask out any regions within the area shown in Fig. 1. We chose to use the Automatic Aperture Magnitudes (AAM) instead of the Corrected Isophotal Magnitudes (CIM), since the latter proved unstable. As well AAM as CIM are intended to give an estimate of the total flux of an object. The AAM is measured using an elliptical aperture with minor axis $b = 2.5 r_1 \epsilon$ and major axis $a = 2.5\frac{r_1}{\epsilon}$, where r_1 is the first moment of the light distribution and ϵ is the ellipticity.

The resulting number of galaxies in the galaxy catalog is 1346 with 456 in the WF2 field, 530 in the WF3 field and 360 in the WF4 field.

As zero-points for the photometry we use those released by the STScI with the WFPC2 HDF-S data for the VEGAMAG system. In the following we shall refer to the F606W and F814W as R and I respectively. Fig. 2 compares the galaxy counts for HDF-N and HDF-S. It is seen that the distributions are similar. In particular, the magnitude bins at which the number counts drop significantly due to incompleteness in the two samples are almost identical. The basic properties of the galaxy catalogs from the two fields as well as from other fields to be discussed below, are listed in Table 1.

2.2. Correlation function from the HDF south catalog

We extract from the galaxy catalog eight R-magnitude-limited samples with limiting magnitudes from R=25.5 to R=29.0 in 0.5 mag steps. As for the HDF-N, galaxies brighter than R=23 are excluded.

The angular correlation function $w(\theta)$ is estimated using the optimal estimator described by Landy & Szalay (1993) :

$$w(\theta) = \frac{DD - 2DR + RR}{RR}, \quad (1)$$

where DD is the number of galaxy-galaxy pairs, DR the number of galaxy-random pairs and RR the number of random-random pairs at the separation θ. We generate a set of 32000 random points distributed according to the Poisson distribution. The number of galaxy-random pairs and random-random pairs at a given magnitude limit are normalized to the total number of galaxy-random and random-random pairs respectively. The errors are calculated from Poisson statistics.

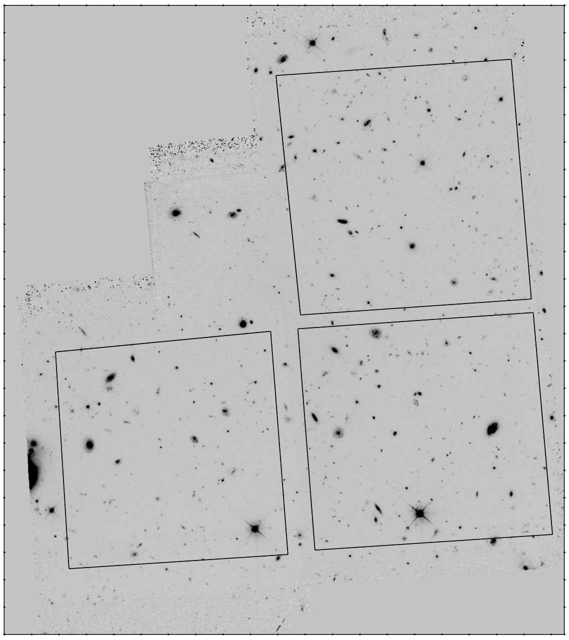

Fig. 1. The WFPC2 HDF-S field showing the the used areas of each of the three Wide Field camera CCDs.

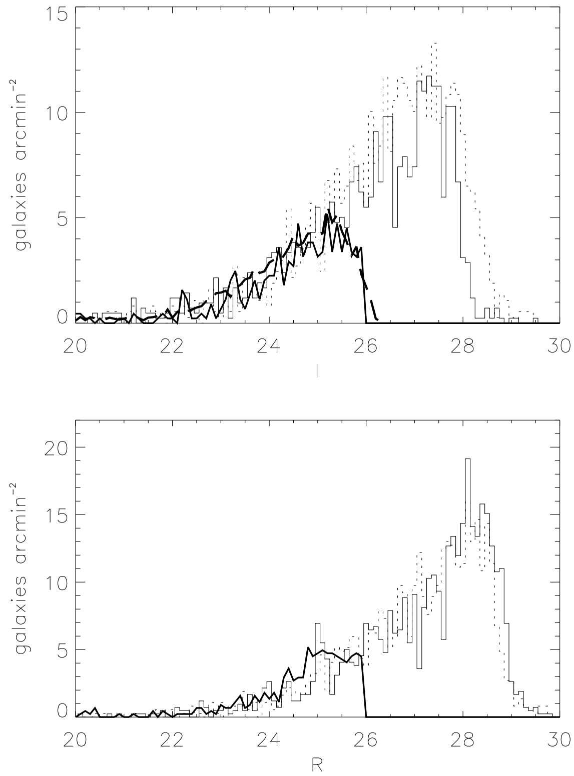

Fig. 2. Comparison of the galaxy counts in 0.1mag bins in the HDF-N and HDF-S fields in the I and R bands. The solid histogram shows the counts for HDF-N and the dashed histogram shows the counts in HDF-S. In the top plot the fat long dashed line shows the galaxy counts in the HDF flanking fields and the fat solid line the counts in NTT SUSI Deep Field. The fat solid line in the lower plot shows the galaxy counts for the NTT SUSI Deep Field.

Since the mean density of galaxies has to be estimated from the sample itself, the integral of the correlation function over the survey area is forced to zero. This reduces the correlation $w(\theta)$ function by an amount C given by the integral :

$$C = \frac{1}{\Omega^2} \iint d\Omega_1 \, d\Omega_2 \, w(\theta), \tag{2}$$

where Ω is the solid angle of the survey area. C is commonly referred to as the 'integral constraint'. Assuming that $w(\theta)$ is a power law,

$$w(\theta) = A\theta^{-\gamma+1}, \quad \gamma = 1.8\,, \tag{3}$$

then $C = 0.078(0.077, 0.080)A$ for the used parts of the WF2(WF3,WF4) area shown in Fig.1.

Fig.3 shows the observed $w(\theta)$ for the eight magnitude limits. The error bars represent 1 σ Poisson errors. The amplitude of $w(\theta)$ is determined by fitting

$$w(\theta) = A\theta^{-\gamma+1} - C, \quad \gamma = 1.8\,, \tag{4}$$

which takes into account the integral constraint.

2.3. Flanking fields

The high resolution deep images of HDF fields are uniquely suited to investigate the correlation function at the faintest magnitudes. However, their small field of view includes too few brighter galaxies to provide useful overlap with ground based measurements of the correlation function. This situation can be improved by taking advantage of the HDF "flanking fields". These fields are contiguous to the HDF fields proper and have been taken during the HDF observing campaigns. We use the two deepest of the HDF-N flanking fields and the nine HDF-S flanking fields.

The HDF proper fields were chosen to avoid bright galaxies. It could be argued that this choice biases the measured correlation amplitude (Brainerd & Smail 1998). As the flanking fields have been chosen with proximity to the HDF fields as the only criterion, no bias related to the HDF proper field is present.

The flanking fields were only imaged with the F814W filter. There is a total of 14 fields. Three of the southern fields contained very bright stars. Rather than masking out these stars we decided not to use these frames in the analysis. Catalogs from the remaining 11 fields were generated in the same manner as for the HDF-S field. The average number counts as a function of magnitude are shown in the upper plot in Fig. 2. For magnitudes up to an I magnitude of about 25 the number per area is consistent with the one in the deep fields. The larger area therefore increases the sample in the brighter magnitude bins

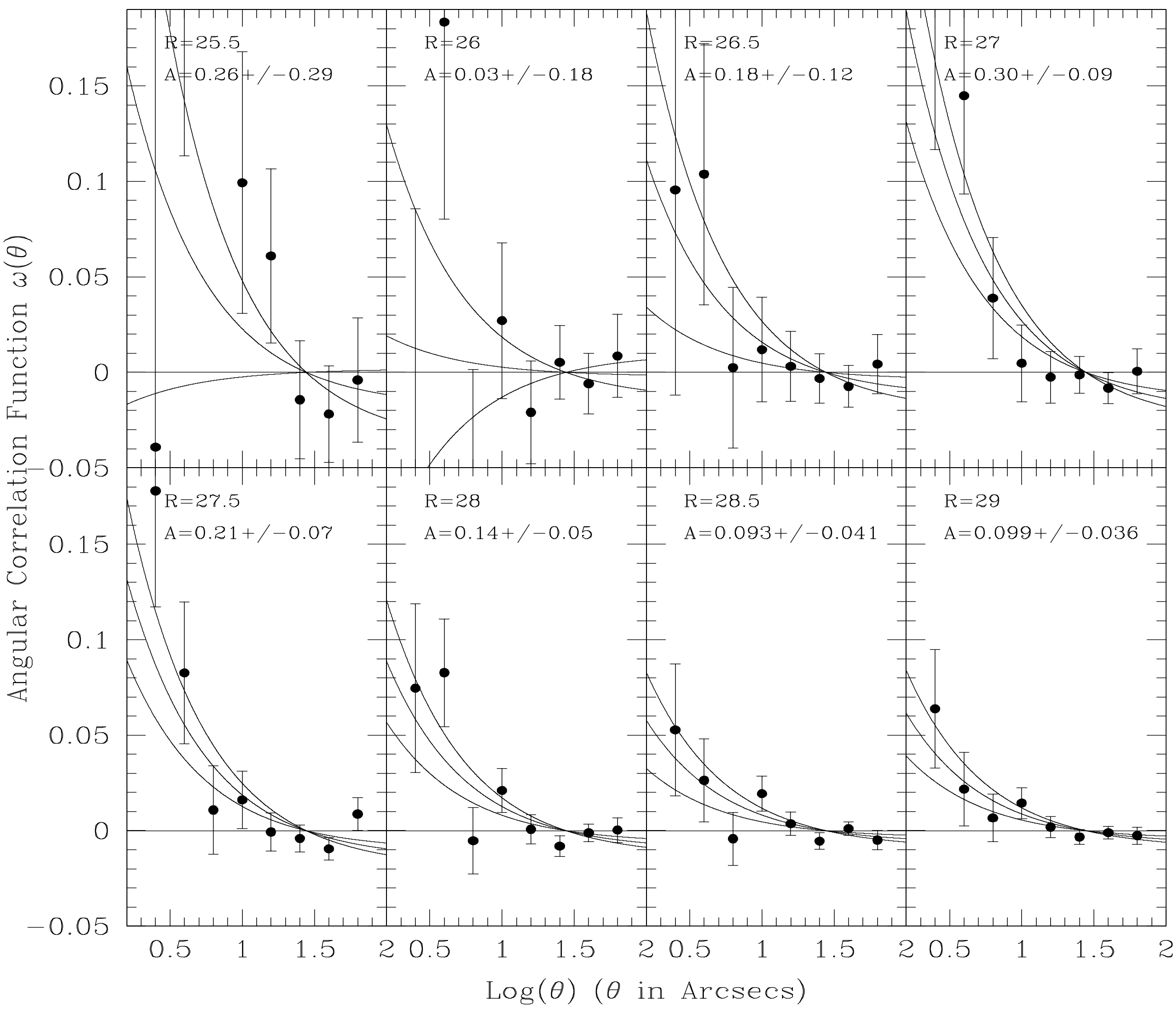

Fig. 3. The measured angular correlation function for the eight magnitude bins. The limiting magnitude for each bin has been indicated on each plot. Also shown is the best fit to a function of the form given in Eq. (4) and the plus and minus 1σ fits.

by almost an order of magnitude. The relevant parameters are again summarized in Table 1.

Finally, we measure the two point correlation function in the three bins 23 <I< 24.5, 23 <I< 25.0, and 23 <I< 25.5 in the same way as described in Sect. 2.2.

2.4. The correlation function from the combined Hubble Deep Fields

In Fig.4 we compare the HDF-S R band results with the results derived by VFC for the HDF-N. The triangles with 1σ error bars show the results for the HDF-S and the squares with 1σ error bars show the results from the HDF-N. For all magnitude bins the measurements from the two fields agree within 1σ. We conclude that any differences are due to random fluctuations, and therefore combine all the available data from the HDF-N and HDF-S projects to obtain our final estimate of the correlation amplitudes from the HDF fields. In Fig.5 we perform the same comparison for the I band, this time also including the measurements from the flanking fields. The measurements are in all bins consistent within 1σ, and we again combine all the available data from the HDF-N and HDF-S projects including the Flanking fields to obtain our final estimate of the I band correlation amplitudes from the HDF fields.

For the R band we determine $w(\theta)$ in the 8 magnitude bins R<25.5, R<26 ..., R<29. In these bins the number counts are not significantly influenced by incompleteness. For the I band we determine $w(\theta)$ in the 8 magnitude bins I<24.5, I<25,...,I<28. The flanking fields are here included in the measurement of $w(\theta)$ in the first three bins.

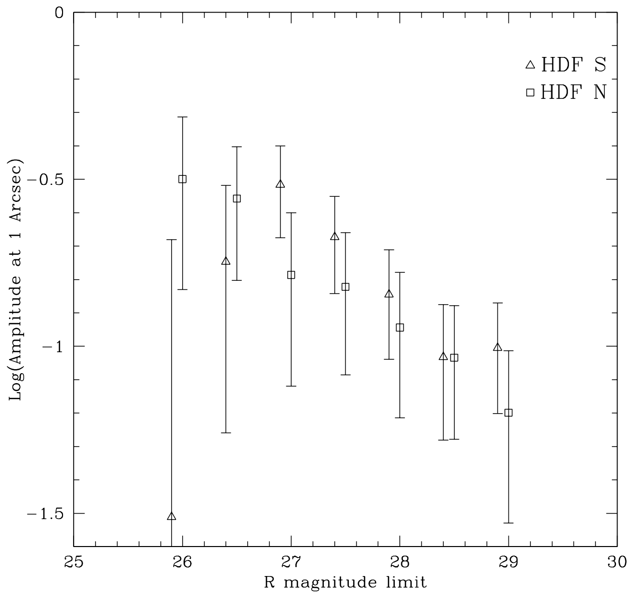

Fig. 4. Comparison for the R band of the amplitude of the angular correlation function in seven magnitude bins for HDF-N (triangles) and HDF-S (squares). The data points for the HDF-S have been shifted 0.1 mag to the left to allow an easier comparison. In all bins do the measurements agree within 1σ.

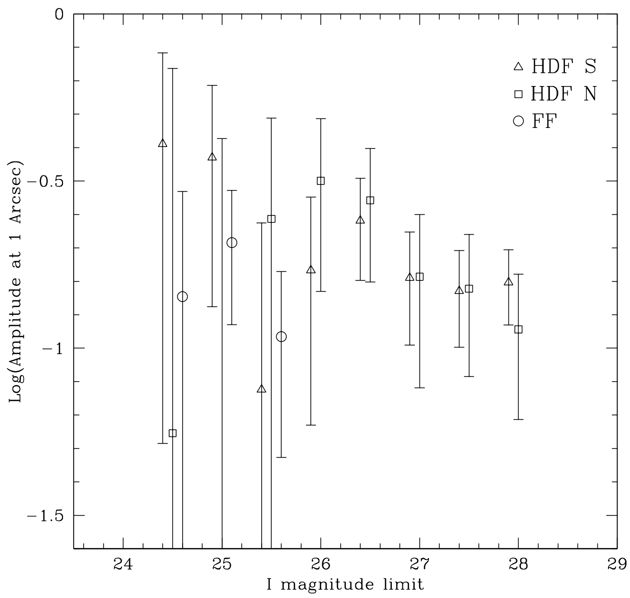

Fig. 5. Comparison for the I band of the amplitude of the angular correlation function for seven magnitude bins for HDF-N (triangles), HDF-S (squares) and for the three first bins also the flanking fields (FF, circles). The data points for the HDF-S have been shifted 0.1 mag to the left and the points for the flanking fields 0.1 mag to the right to allow an easier comparison. In all bins do the measurements agree within 1σ.

The determination of $w(\theta)$ and the power law fit is done as described in Sect. 2.2. We detect a positive correlation amplitude in all 8 bins in both R and I.

3. The ESO-NTT deep field

In order to verify that the correlation amplitudes we measured in the HST WFPC2 frames are not in some way due to properties of the WFPC2 instrument or HDF observing or reduction procedure, it is desirable to compare to a catalog of galaxies derived from deep high-resolution ground based observations. The ESO-NTT field (Arnouts et al. 1999), for which the images are publicly available, is suitable for this purpose. A catalog of galaxies for this field has been provided by S. D'Odorico at the ESO website at http://www.eso.org/ndf. The field provides deep multi-colour imaging taken with good sampling of the PSF. The depth of the images is about 26.7 in R and 26.3 in I. The effective seeings of the co-added images are about 0.7-0.8 arcsec.

We determine the amplitude of $w(\theta)$ in the magnitude intervals 22–24.5, 22–25.0 and 22–25.5 for both the I and R filters. We use an area of 4.4 arcmin^2 confined by the pixel values 40 <x,y< 1020 (chosen to avoid edge-effects). For this area we derive an integral constraint of $C = 0.0468A$. Due to the small size of the NTT SUSI Deep Field we cannot determine the amplitude of $w(\theta)$ very precisely. Nevertheless, we do detect a positive correlation signal in all but one of the magnitude bins. The measured amplitudes of $w(\theta)$ are in all bins consistent with the measurements in the two HDFs within 1σ (see Fig. 6 and Fig. 7).

Stellar contamination of the sample can reduce the measured correlation amplitude. For a sample with a fraction $f_{\rm star}$ of galaxies, the measured correlation amplitude is reduced by a factor $\propto (1 - f_{\rm star})^{-2}$. Fortunately, the excellent seeing allows a firm galaxy/star discrimination. We follow Arnouts et al. in classifying as stars all objects with SExtractor classifier larger than 0.9 in the I band. This procedure removes about 5% of the objects in the field. For objects fainter than 24 the SExtractor classifier is not efficient, so we assume conservatively that about 5% of the objects used to measure the correlation amplitude are stars. In fact, the star counts are shallower at faint magnitudes than that of galaxies (Reid et al. 1996, their Fig. 1), which means that the star fraction at $I > 24$ must be smaller than for $I < 24$. Therefore, a conservative upper limit of the error introduced by stellar contamination of the catalog is 10%, which is significantly smaller than the random uncertainties.

4. The correlation amplitude as a function of magnitudes

The correlation amplitudes presented above overlap neither in magnitude nor scale with most such measurements from ground based data. Investigations of the correlation amplitude as a function of magnitudes which use these data therefore require knowledge of the power law index δ in order to compare amplitudes measured at different separations. The HST data presented here are consistent with the usual $\delta = 0.8$ power law for angular separations between 1 arcsec and 1 arcmin, but do not rule out steeper of flatter slopes. On the other hand, ground based data have been used to derive the shape of the correlations function at separations between 0.5 and 5 arcminutes (e.g. Postman et al. 1998), but it is not clear whether the slopes can be extrapolated to smaller separations. In the following investigation, we have adopted a slope of 0.8 in most cases. The uncertainty in the slope is probably the largest source of uncertainty in the comparison of measurements from different surveys.

Fig. 6 shows the measured amplitudes of $w(\theta)$ at 1 arcsec as a function of the limiting magnitudes of surveys in the R band from measurements by Brainerd et al. (1995), Roche et al. (1993), Couch et al. (1993) and Woods & Fahlman (1997). Where necessary (data from Roche et al. and Couch et al.), we have scaled original correlation amplitudes quoted in each paper to the amplitude at 1 arcsec by assuming a power law for the correlation function with $\delta = 0.8$. Similarly, Fig. 7 shows the measured amplitudes of $w(\theta)$ at 1 arcsec as a function of the limiting magnitudes of the surveys in the I band. The measurements of Postman et al. (1998), Brainerd & Smail (1998), Woods & Fahlman (1997), Benoist et al. (1999), Benoist et al. (in prep.) and Lidman & Peterson (1996) are included. Here, all the amplitudes except those from Woods & Fahlman (1997) and Postman et al. (1998) were extrapolated to a separation of 1 arcsec with $\delta = 0.8$. For the Postman et al. (1998) measurements, the data at 1 arcmin and 0.5 arcmin were extrapolated using the slope measured by the authors in the range 0.5 arcmin – 5 arcmin.

Both in Fig. 6 and Fig. 7, we show theoretical predictions of the expected correlation amplitudes. The models are identical to those shown by VFC, but with the assumed redshift distribution in the faint magnitude bins derived from the photometric redshift distribution of HDF-N galaxy by Fernández-Soto et al. (1999). The median redshifts adopted at magnitudes brighter than 26 in the R band are the same as those used by VFC. The models are specified by a present clustering length r_0 and and evolution parameter ϵ (see VFC for details). The models shown have a present clustering length of $r_0 = 4.0h^{-1}$ Mpc and assume no evolution of clustering (dotted line, ϵ=0), linear evolution of clustering (solid line, ϵ=0.8) or non-linear evolution of clustering (dashed line, ϵ=1.6).

Several data sets shown in Fig. 6 and Fig. 7 are in conflict with each other at the 5-7σ level. This reflects the fact that the main source of errors are systematic errors, while the error bars in most cases only include statistical errors. In particular at faint magnitudes, systematic uncertainties are hard to quantify. The disagreements appear to be larger in the I-band. This might be due to the fact that in the I band, variations in the effective filter bandpasses result in relatively large differences in the redshift distribution of extracted galaxy samples. Also, the limiting magnitude on the abscissa is somewhat depending on the limiting magnitudes at the *bright* end. However, as the galaxy counts (N) increases steeply with the limiting magnitude at the faint end (mag$_{lim}$, $\log N \propto 0.6$ mag$_{lim}$), the uncertainty due to different limiting magnitudes is small (the difference in the median magnitude of two galaxy samples with limiting magnitude 25 at the faint end and limiting magnitudes at the bright end of 20 and 24 is only about 0.5mag). More likely, however, the disagreement is related to the extrapolation from 1 arcmin scales to 1 arcsec scales. In Postman et al. (1998, their Table 3) it can be seen that the power δ seem to decline at $I > 21$ to smaller values than the canonical value 0.8 ($\delta = 0.7$ at $I = 22$ and $\delta = 0.5$ at $I = 23$), especially at the smallest scales 0.5 arcsec $< \theta <$ 5 arcmin. A similar trend was noted by Benoist et al. (1999). Brainerd & Smail (1998) find at best fitting value of $\delta = 0.7$ at $I > 24.5$. A change in slope from $\delta = 0.8$ to $\delta = 0.5$ amounts to factor of 3.4 difference in the extrapolation from 1 arcmin scales to 1 arcsec scales. Due to these uncertainties, our current knowledge of the amplitude and shape of the correlation function in the range 1 arcmin $< \theta <$ 1 arcsec at the faintest magnitude limits reachable from the ground, I=23–25, is unfortunately still poor.

5. Summary and conclusions

From the data presented above we can draw the following conclusions.

- The clustering amplitudes measured in the HDF-N field have been confirmed with the independent sample from the Southern HDF. This rules out that the low amplitudes measured in the HDF-N field are due to some cosmological fluctuations. The HDF-N field seems to provide a fair sample of high-redshift galaxies.
- The clustering in the HDF flanking fields is consistent with the one measured from ground based samples at the bright end of the magnitude range, and with the ones measured in the HDFs at the faint end. This provides additional support to the view that the HDF fields represent indeed a fair view of the high-redshift universe.
- The measured correlation amplitudes in the ESO-NTT galaxy sample in magnitude bins which overlap those of the HDF sample are consistent with the HDF measurements. This observation verifies that correlations measured with WFPC2 are not due to some instrumental effects.
- The results plotted in Fig. 6 show a continuous decline of the amplitude of the correlation function in R. We do not confirm the Brainerd & Smail (1998) detection of a flattening in the I band at I=22–23.
- There is some indication of a flattening of the correlation amplitudes at the faintest levels ($R \approx 27$ or $I \approx 26$). Using models for the redshift distribution, VFC interpreted this flattening as evidence for linear evolution of the clustering of a galaxy population which at present has a correlation length of about $4h^{-1}$Mpc. The data presented in this paper are still in good agreement with this interpretation.
- Interpretation of Fig. 6 and 7 is difficult given the significant disagreement between data points from different studies. This disagreement could be caused by a change of δ as a function of magnitude and scale. To reach a final understanding of the two-point correlation function data compiled in this work, it therefore appears to be essential first

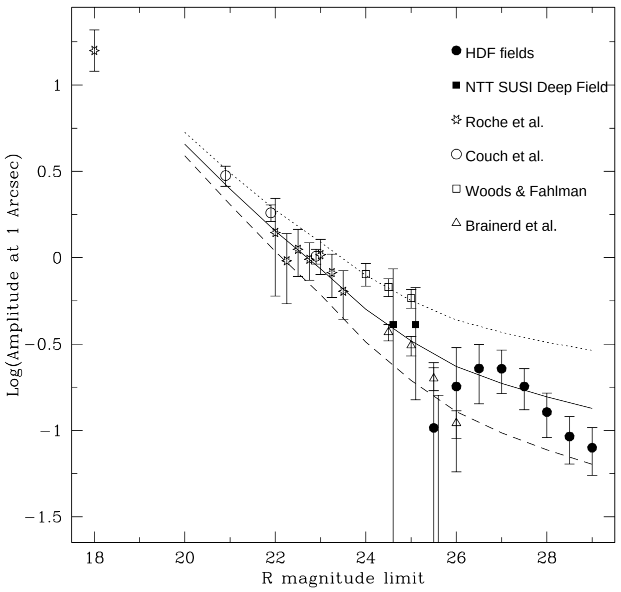

Fig. 6. The amplitude of $w(\theta)$ at 1 arcsec as a function of the limiting R band magnitude for a number of ground based surveys and the measurements from the Hubble Deep fields presented in this paper. The superimposed curves are theoretical predictions for a population of galaxies with a present clustering length of $r_0 = 4.0h^{-1}$ Mpc and assuming no evolution of clustering (dotted line), linear evolution (solid line) as well as non-linear evolution of clustering (dashed line).

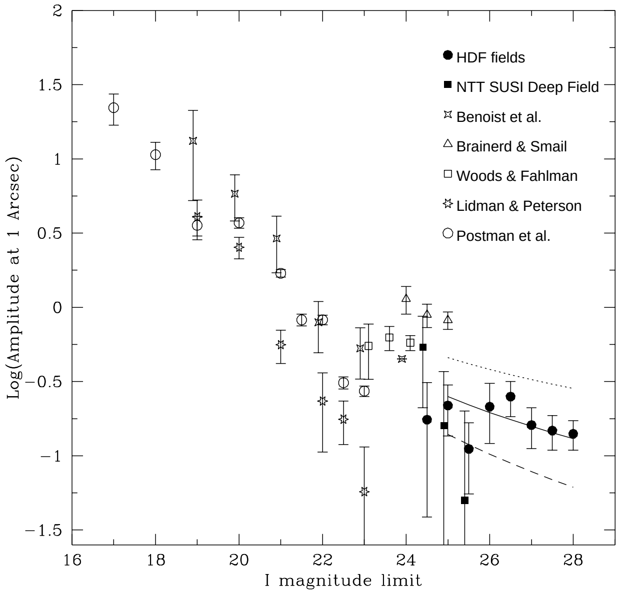

Fig. 7. The amplitude of $w(\theta)$ at 1 arcsec as a function of the limiting I band magnitude for a number of ground based surveys and the measurements from the Hubble Deep fields presented in this paper. The superimposed curves are again the models with a present clustering length of $r_0 = 4.0h^{-1}$ Mpc and assuming no evolution of clustering (dotted line), linear evolution (solid line) as well as non-linear evolution of clustering (dashed line).

to understand the detailed behavior of the *shape* of the correlation function.

Acknowledgments

We wish to thank C. Benoist and B. Thomsen for helpful discussions and C. Benoist for giving giving us access to some of his results from the EIS data prior to publication. We thank S. D'Odorico for making available the catalog from the NTT Deep Field. We thank the referee, T. Brainerd, for comments which significantly improved the manuscript. This work made use of the ESO/ST-ECF Science Archive Facility.

References

Arnouts S., D'Odorico S., Cristiani S., Fontana A., Giallongo E., 1999, A&A 341, 641
Benoist C., da Costa L.N., Olsen L.F., et al., 1999, A&A 346, 58
Bertin E, Arnouts S, 1996, A&AS 117, 393
Brainerd T.G., Smail I., 1998, ApJ 496, L137
Brainerd T. G., Smail I. R., Mould J.R., 1995, MNRAS 275, 781
Clements D.L., Couch W.J., 1996, MNRAS 280, 43L
Colley W.N., Rhoads J.E., Ostriker J.P., Spergel, D.N., 1996, ApJ 473, L63
Couch W.J., Jurcevic J.S., Boyle B.J., 1993, MNRAS 260, 241
Fernández-Soto A., Lanzetta K.M., Yahil A. 1999, ApJ 513, 34
Landy S.D., Szalay A.S., 1993, ApJ 412, 64
Le Fèvre O., Hudon D., Lilly S.J., et al., 1996, ApJ 460, L1
Lidman C.E., Peterson B.A., 1996, MNRAS 279, 1357
Postman M., Lauer T.R., Szapudi I., Oegerle W., 1998, ApJ 506, 33
Reid I.N., Yan L., Majewski S., Thompson I., Smail I., 1996, AJ 112, 1472
Roche N., Shanks T., Metcalfe N., Fong R., 1993, MNRAS 263, 360
Villumsen J.V., Freudling W., da Costa L.N., 1996, ApJ 481, 578 (VFC).
Williams R.E., Brett B., Dickinson M., et al., 1996, AJ 112, 1335
Williams R.E., Baum S.A., Bergeron L.E., et al., 1998, AAS 193, 7501
Woods D., Fahlman G.G., 1997, ApJ 490, 11